Weierstraß-Institut
für Angewandte Analysis und Stochastik
Leibniz-Institut im Forschungsverbund Berlin e. V.

Preprint ISSN 0946 – 8633

Stability of explicit Runge–Kutta methods for finite element approximation of linear parabolic equations on anisotropic meshes

Weizhang Huang[1], Lennard Kamenski[2], Jens Lang[3]

submitted: November 21, 2013

[1] The University of Kansas
Department of Mathematics
Lawrence, KS 66045
US
email: whuang@ku.edu

[2] Weierstrass Institute
Mohrenstr. 39
10117 Berlin
Germany
email: lennard.kamenski@wias-berlin.de

[3] Technische Universität Darmstadt
Fachbereich Mathematik
Graduiertenschule Computational Engineering
Center of Smart Interfaces
Dolivostr. 15, 64293 Darmstadt, Germany
email: lang@mathematik.tu-darmstadt.de

No. 1869

Berlin 2013

2010 *Mathematics Subject Classification.* 65M60, 65M50, 65F15.

Key words and phrases. finite element method, anisotropic mesh, stability condition, parabolic equation, explicit Runge-Kutta method.

Lennard Kamenski is thankful to Klaus Gärtner for comments that lead to Remark 2.2 and to Larissa Kaspar for the code used in computation in Example 4.3. Supported in part by the NSF (U.S.A.) under Grant DMS-1115118, the DFG (Germany) under Grant KA 3215/2-1, the Excellence Initiative of the German Federal and State Governments, and the Graduate School of Engineering at the TU Darmstadt.

Edited by
Weierstraß-Institut für Angewandte Analysis und Stochastik (WIAS)
Leibniz-Institut im Forschungsverbund Berlin e. V.
Mohrenstraße 39
10117 Berlin
Germany

Fax: +49 30 20372-303
E-Mail: preprint@wias-berlin.de
World Wide Web: http://www.wias-berlin.de/

Abstract

We study the stability of explicit Runge-Kutta integration schemes for the linear finite element approximation of linear parabolic equations. The derived bound on the largest permissible time step is tight for any mesh and any diffusion matrix within a factor of $2(d+1)$, where d is the spatial dimension. Both full mass matrix and mass lumping are considered. The bound reveals that the stability condition is affected by two factors. The first one depends on the number of mesh elements and corresponds to the classic bound for the Laplace operator on a uniform mesh. The other factor reflects the effects of the interplay of the mesh geometry and the diffusion matrix. It is shown that it is not the mesh geometry itself but the mesh geometry in relation to the diffusion matrix that is crucial to the stability of explicit methods. When the mesh is uniform in the metric specified by the inverse of the diffusion matrix, the stability condition is comparable to the situation with the Laplace operator on a uniform mesh. Numerical results are presented to verify the theoretical findings.

1 Introduction

Adaptive meshes are commonly used for the numerical solution of partial differential equations (PDEs) to enhance computational efficiency but there are still lacks in the mathematical understanding of the effects of the variation of element size and shape on the properties of numerical schemes used for solving PDEs. In this paper, we are concerned with the stability of explicit Runge-Kutta time integration of linear finite element approximation with general nonuniform simplicial meshes for the initial-boundary value problem (IBVP)

$$\begin{cases} \partial_t u = \nabla \cdot (\mathbb{D}\nabla u)\,, & \boldsymbol{x} \in \Omega, \quad t \in (0,T]\,, \\ u(\boldsymbol{x},t) = 0, & \boldsymbol{x} \in \Gamma_D, \quad t \in (0,T]\,, \\ \mathbb{D}\nabla u(\boldsymbol{x},t)\cdot \boldsymbol{n} = 0, & \boldsymbol{x} \in \Gamma_N, \quad t \in (0,T]\,, \\ u(\boldsymbol{x},0) = u_0(\boldsymbol{x}), & \boldsymbol{x} \in \Omega \end{cases} \tag{1}$$

where $\Omega \subset \mathbb{R}^d$ $(d \geq 1)$ is a bounded polygonal or polyhedral domain, $\Gamma_D \cup \Gamma_N = \partial\Omega$, Γ_D has a positive $(d-1)$-volume, u_0 is a given initial function, and $\mathbb{D}$ is the diffusion matrix which is always assumed to be symmetric and uniformly positive definite on Ω. In this study, we also assume that $\mathbb{D}$ is time independent, i.e., $\mathbb{D} = \mathbb{D}(\boldsymbol{x})$.

Assume that $u_0 \in H^1_D(\Omega) = \{v \in H^1(\Omega) : v = 0 \text{ on } \Gamma_D\}$. Then, if u is sufficiently smooth, we have the stability estimates

$$\begin{cases} \|u(\cdot,t)\|_{L^2(\Omega)} \leq \|u_0\|_{L^2(\Omega)}, & t \in (0,T]\,, \\ |||u(\cdot,t)|||_{H^1(\Omega)} \leq |||u_0|||_{H^1(\Omega)}, & t \in (0,T]\,, \end{cases} \tag{2}$$

where $|||u(\cdot,t)|||_{H^1(\Omega)} \equiv \|\mathbb{D}^{1/2}\nabla u\|_{L^2(\Omega)}$ is the energy norm of $u(\cdot,t)$. It is essential that a numerical scheme applied to (1) has similar stability estimates. The stability of the time integration depends on the largest eigenvalue of the system related to the numerical scheme which, in turn, depends on the underlying meshes and the coefficients of the IBVP. For a uniform mesh and the Laplace operator, it is well known that the largest permissible time step is proportional to the square of the element diameter. In the case of a nonuniform mesh or a variable diffusion matrix the situation becomes more complicated. Essentially, one needs to estimate the largest eigenvalues of $M^{-1}A$, where M and A are the mass and stiffness matrices corresponding to the discretization of the IBVP. This can be done by estimating the extreme

eigenvalues of M and A. Tight bounds on those of the mass matrix M for linear finite elements with locally quasi-uniform meshes are available in the literature and typically proportional to the extremal mesh element volumes [Fri73; GM06; Wat87], whereas those for the stiffness matrix A are more difficult to obtain and only a few results are available in the literature for the case of nonuniform meshes. For example, Fried [Fri73] shows how to obtain these bounds for the finite element approximation of the Laplace operator for general nonuniform meshes using local element mass and stiffness matrices. Graham and McLean [GM06] study the finite/boundary element approximation of a general differential/integral operator on locally quasi-uniform meshes in terms of patch volumes and aspect ratios. Du, Wang, and Zhu [DWZ09] obtain bounds on the extreme eigenvalues of the stiffness matrix for the Galerkin approximation of a general diffusion operator in terms of element geometry. Zhu and Du [ZD11; ZD14] further develop bounds on the largest permissible time step for time dependent problems. It is worth mentioning that these existing works allow anisotropic meshes. However, the interplay between the mesh geometry and the diffusion matrix is not really taken into account. As we will see in the current work, this interplay is crucially important for the stability of explicit integration schemes (see Remark 3.2 and Example 4.4 for details and a numerical example). Moreover, the existing analysis either employs some mesh regularity assumptions such as the local uniformity or involves parameters related to mesh regularity such as the maximum ratio of volumes of neighboring elements and/or the maximum number of elements in a patch in final estimates.

The objective of this paper is to develop estimates for the permissible time step which are accurate and tight for *any mesh* and *any diffusion matrix*. We shall utilize the bounds recently obtained by Kamenski, Huang, and Xu [KHX] on the extreme eigenvalues of M and the largest eigenvalue of A for a general diffusion operator with arbitrary meshes. The developed stability condition that is expressed in terms of matrix entries is tight within a constant factor independent of the mesh and the diffusion matrix, and no assumption on the mesh regularity is made in the development. Moreover, we shall show that the alignment of the mesh with the diffusion matrix plays a crucial role in the stability condition: the largest permissible time step depends only on the number of mesh elements and the mesh geometry in relation to the diffusion matrix. In particular, when a mesh that is uniform in the metric specified by $\mathbb{D}^{-1}$ is used, the stability condition is essentially the same as that for the Laplace operator with a uniform mesh.

The paper is organized as follows. We start in Sect. 2 with the problem setting and a detailed description of mesh quality measures which are needed for the geometric interpretations of stability estimates. The main results on stability are given in Sect. 3; both the full mass matrix and mass lumping are considered. Numerical examples to demonstrate the theoretical findings are presented in Sect. 4, including a two-dimensional ground water flow problem. Conclusions are drawn in Sect. 5.

2 Linear finite element approximation

We consider the standard linear finite element method for the spatial discretization of IBVP (1).

We assume that a family of simplicial meshes, $\{\mathcal{T}_h\}$, is given for Ω. While having adaptive meshes in mind, we consider the meshes to be general nonuniform ones, which may contain elements of small size and large aspect ratio. Let K be an arbitrary element of $\mathcal{T}_h$, $\hat{K}$ the *reference element*, and ω_i the element *patch* of the i^{th} vertex (Fig. 1). Element and patch

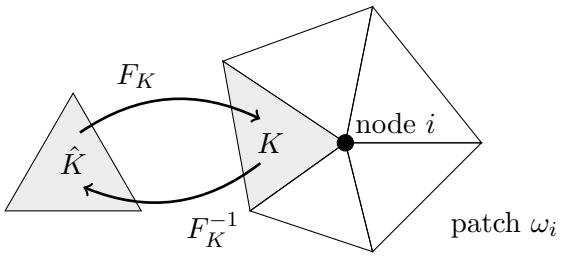

Figure 1: Reference and mesh elements, mapping F_K, i^{th} node and its patch ω_i.

volumes are denoted by

$$|K| \quad \text{and} \quad |\omega_i| = \sum_{K \in \omega_i} |K|.$$

For each mesh element $K \in \mathcal{T}_h$ let F_K be the invertible affine mapping from $\hat{K}$ to K (Fig. 1) and F'_K its Jacobian matrix. Note that F'_K is a constant matrix with $\det(F'_K) = |K|$ (for simplicity, we assume that $\hat{K}$ is equilateral with $|\hat{K}| = 1$).

Let V^h be the linear finite element space associated with mesh $\mathcal{T}_h$. Defining $V_D^h = V^h \cap H_D^1(\Omega) = \{v^h \in V^h : v^h = 0 \text{ on } \Gamma_D\}$, the piecewise linear finite element solution $u^h(t) \in V_D^h$, $t \in (0, T]$ is defined by

$$\int_\Omega v^h \partial_t u^h \, d\boldsymbol{x} = -\int_\Omega \nabla v^h \cdot \mathbb{D} \nabla u^h \, d\boldsymbol{x}, \qquad \forall v^h \in V_D^h, \quad t \in (0, T], \tag{3}$$

subject to the initial condition

$$\int_\Omega u^h(\boldsymbol{x}, 0) v^h \, d\boldsymbol{x} = \int_\Omega u_0(\boldsymbol{x}) v^h \, d\boldsymbol{x}, \qquad \forall v^h \in V_D^h. \tag{4}$$

We denote the number of the elements of $\mathcal{T}_h$ by N and the number of the interior vertices plus the vertices associated with the Neumann boundary condition by N_{vi}. If we express u^h as

$$u^h(\boldsymbol{x}, t) = \sum_{j=1}^{N_{vi}} u_j^h(t) \phi_j(\boldsymbol{x}),$$

where ϕ_j is the linear basis function associated the j^{th} vertex ($j = 1, \ldots, N_{vi}$), from (3) and (4) we obtain

$$M \boldsymbol{U}_t = -A \boldsymbol{U}, \quad \boldsymbol{U}(0) = \boldsymbol{U}_0, \tag{5}$$

where $\boldsymbol{U} = (u_1^h, \ldots, u_{N_{vi}}^h)^T$ and M and A are the mass and the stiffness matrices,

$$M_{ij} = \int_\Omega \phi_i \phi_j \, d\boldsymbol{x}, \quad \text{and} \quad A_{ij} = \int_\Omega \nabla \phi_i \cdot \mathbb{D} \nabla \phi_j \, d\boldsymbol{x}, \qquad i, j = 1, \ldots, N_{vi}. \tag{6}$$

We shall investigate how the geometry of the mesh and the anisotropy of the diffusion matrix affect the stability of explicit Runge-Kutta methods for integrating (5). In the following we assume that the mesh is fixed for all time steps.

2.1 Mathematical description of nonuniform meshes; mesh quality measures

It is known [Hua05b] that an adaptive mesh, which is typically nonuniform, can be generated as a uniform mesh in the metric specified by a given metric tensor (which is always assumed to be symmetric and uniformly positive definite in Ω). Moreover, for any given mesh a metric tensor can be defined such that the mesh is uniform in the metric specified by this tensor [HR11]. Thus, it is natural to consider nonuniform meshes in relation to a given metric tensor. In the following, we describe several quality measures and mathematical characterizations for (nonuniform) meshes in terms of a given metric tensor, $\mathbb{M} = \mathbb{M}(\boldsymbol{x})$. As will be seen in Sect. 3, the matching between the mesh metric tensor and the diffusion matrix plays a crucial role for the stability condition. In our analysis, we slightly adjust the original definitions of those mesh quality measures in [Hua05a] (see also [Hua07; HR11]).

Let

$$\mathbb{M}_K = \frac{1}{|K|}\int_K \mathbb{M}\, d\boldsymbol{x}, \qquad |K|_{\mathbb{M}} = |K|\det(\mathbb{M}_K)^{\frac{1}{2}}, \qquad |\Omega|_{\mathbb{M},h} = \sum_{K\in\mathcal{T}_h} |K|_{\mathbb{M}}. \tag{7}$$

Note that $\mathbb{M}_K$ is the average of $\mathbb{M}$ over element K and $|K|_{\mathbb{M}}$ and $|\Omega|_{\mathbb{M},h}$ are approximate volumes of K and Ω in the metric $\mathbb{M}$, viz.,

$$|K|_{\mathbb{M}} \approx \int_K \det\big(\mathbb{M}(\boldsymbol{x})\big)^{\frac{1}{2}}\, d\boldsymbol{x}, \qquad |\Omega|_{\mathbb{M},h} \approx \sum_{K\in\mathcal{T}_h}\int_K \det\big(\mathbb{M}(\boldsymbol{x})\big)^{\frac{1}{2}}\, d\boldsymbol{x} = |\Omega|_{\mathbb{M}}.$$

Hereafter, without confusion we will call $|K|_{\mathbb{M}}$ and $|\Omega|_{\mathbb{M},h}$ the volumes of K and Ω in the metric $\mathbb{M}$, respectively. We also define the *average diameter* of element K and the *global average element diameter* with respect to $\mathbb{M}$ as

$$h_{K,\mathbb{M}} = |K|_{\mathbb{M}}^{\frac{1}{d}}, \qquad h_{\mathbb{M}} = \left(\frac{1}{N}|\Omega|_{\mathbb{M},h}\right)^{\frac{1}{d}}.$$

Recall that the diameter of K, h_K, is defined as the length of the longest edge of K.

With these notations, we now are ready to describe the mesh quality measures. The first one, the *equidistribution* quality measure, is defined as the ratio of the average element volume to the volume of K, both measured in the metric specified by $\mathbb{M}_K$,

$$\mathrm{Q}_{\mathrm{eq},\mathbb{M}}(K) = \frac{\frac{1}{N}|\Omega|_{\mathbb{M},h}}{|K|_{\mathbb{M}}} = \left(\frac{h_{\mathbb{M}}}{h_{K,\mathbb{M}}}\right)^d. \tag{8}$$

It satisfies

$$0 < \mathrm{Q}_{\mathrm{eq},\mathbb{M}}(K) < \infty, \qquad \frac{1}{N}\sum_{K\in\mathcal{T}_h}\frac{1}{\mathrm{Q}_{\mathrm{eq},\mathbb{M}}(K)} = 1, \qquad \max_{K\in\mathcal{T}_h}\mathrm{Q}_{\mathrm{eq},\mathbb{M}}(K) \geq 1. \tag{9}$$

The second one, the *alignment* quality measure, is local (elementwise) and measures how closely the principal directions of the circumscribed ellipsoid of K are aligned with the eigenvectors of $\mathbb{M}_K$ and the semi-lengths of the principal axes are inversely proportional to the square root of the eigenvalues of $\mathbb{M}_K$. It is defined as

$$\mathrm{Q}_{\mathrm{ali},\mathbb{M}}(K) = \frac{\left\|(F_K')^{-1}\mathbb{M}_K^{-1}(F_K')^{-T}\right\|_2}{\det\left((F_K')^{-1}\mathbb{M}_K^{-1}(F_K')^{-T}\right)^{\frac{1}{d}}} = \frac{\left\|(F_K')^{-1}\mathbb{M}_K^{-1}(F_K')^{-T}\right\|_2}{h_{K,\mathbb{M}}^{-2}}. \tag{10}$$

Since

$$\left\|(F_K')^{-1}\mathbb{M}_K^{-1}(F_K')^{-T}\right\|_2 \geq \det\left((F_K')^{-1}\mathbb{M}_K^{-1}(F_K')^{-T}\right)^{\frac{1}{d}},$$

the measure always satisfies

$$1 \leq \mathrm{Q}_{\mathrm{ali},\mathbb{M}}(K) < \infty,$$

with $\mathrm{Q}_{\mathrm{ali},\mathbb{M}}(K) = 1$ if and only if K is equilateral with respect to $\mathbb{M}_K$. The alignment quality measure can be seen as an alternative to the aspect ratio of K in the metric specified by $\mathbb{M}_K$ and it satisfies

$$\mathrm{Q}_{\mathrm{ali},\mathbb{M}}(K) \leq \hat{h}^2 \cdot \left(\frac{h_{K,\mathbb{M}}}{\rho_{K,\mathbb{M}}}\right)^2, \tag{11}$$

where $\hat{h}$ is the length of the longest edge of $\hat{K}$ and $\rho_{K,\mathbb{M}}$ is the diameter of the largest sphere inscribed in the element K viewed in the metric M_K. To show this, we consider two points $\boldsymbol{x}_1, \boldsymbol{x}_2 \in K$ and the corresponding points $\boldsymbol{\xi}_1 = F_K^{-1}(\boldsymbol{x}_1)$ and $\boldsymbol{\xi}_2 = F_K^{-1}(\boldsymbol{x}_2)$ in $\hat{K}$. The distance between $\boldsymbol{x}_1$ and $\boldsymbol{x}_2$ in the metric $\mathbb{M}_K$ is

$$\begin{aligned}
\|\boldsymbol{x}_1 - \boldsymbol{x}_2\|^2_{\mathbb{M}_K} &= (\boldsymbol{x}_1 - \boldsymbol{x}_2)^T \mathbb{M}_K (\boldsymbol{x}_1 - \boldsymbol{x}_2) \\
&= (\boldsymbol{\xi}_1 - \boldsymbol{\xi}_2)^T (F_K')^T \mathbb{M}_K F_K' (\boldsymbol{\xi}_1 - \boldsymbol{\xi}_2) \\
&= \|\boldsymbol{\xi}_1 - \boldsymbol{\xi}_2\|_2^2 \cdot \frac{(\boldsymbol{\xi}_1 - \boldsymbol{\xi}_2)^T}{\|\boldsymbol{\xi}_1 - \boldsymbol{\xi}_2\|_2} (F_K')^T \mathbb{M}_K F_K' \frac{(\boldsymbol{\xi}_1 - \boldsymbol{\xi}_2)}{\|\boldsymbol{\xi}_1 - \boldsymbol{\xi}_2\|_2} \\
&\leq \hat{h}^2 \cdot \frac{(\boldsymbol{\xi}_1 - \boldsymbol{\xi}_2)^T}{\|\boldsymbol{\xi}_1 - \boldsymbol{\xi}_2\|_2} (F_K')^T \mathbb{M}_K F_K' \frac{(\boldsymbol{\xi}_1 - \boldsymbol{\xi}_2)}{\|\boldsymbol{\xi}_1 - \boldsymbol{\xi}_2\|_2}.
\end{aligned}$$

If we take the minimum over all points on the largest sphere inscribed in the element K viewed in the metric M_K, then

$$\rho^2_{K,\mathbb{M}} \leq \hat{h}^2 \lambda_{\min}((F_K')^T \mathbb{M}_K F_K').$$

Hence,

$$\left\|(F_K')^{-1}\mathbb{M}_K^{-1}(F_K')^{-T}\right\|_2 = \frac{1}{\lambda_{\min}((F_K')^T \mathbb{M}_K F_K')} \leq \frac{\hat{h}^2}{\rho^2_{K,\mathbb{M}}}, \tag{12}$$

which, together with (10), gives (11).

The *element quality* measure is defined as a combination of $\mathrm{Q}_{\mathrm{ali},\mathbb{M}}$ and $\mathrm{Q}_{\mathrm{eq},\mathbb{M}}$,

$$\mathrm{Q}_{\mathbb{M}}(K) = \mathrm{Q}_{\mathrm{ali},\mathbb{M}}(K) \cdot (\mathrm{Q}_{\mathrm{eq},\mathbb{M}}(K))^{\frac{2}{d}} = h^2_{\mathbb{M}} \left\|(F_K')^{-1}\mathbb{M}_K^{-1}(F_K')^{-T}\right\|_2. \tag{13}$$

It measures how far K is from being equilateral with unitary volume when viewed in the metric specified by $\mathbb{M}$. By definition and from (12) it follows that

$$0 < \mathrm{Q}_{\mathbb{M}}(K) \leq \hat{h}^2 \left(\frac{h_{\mathbb{M}}}{\rho_{K,\mathbb{M}}}\right)^2 < \infty.$$

When a mesh is uniform with respect to $\mathbb{M}$ (we will refer to it as an $\mathbb{M}$-*uniform* mesh) then it satisfies

$$\mathrm{Q}_{\mathrm{ali},\mathbb{M}}(K) = 1, \qquad \mathrm{Q}_{\mathrm{eq},\mathbb{M}}(K) = 1, \quad \forall K \in \mathcal{T}_h, \tag{14}$$

which is equivalent to

$$\mathrm{Q}_{\mathbb{M}}(K) = 1, \quad \forall K \in \mathcal{T}_h. \tag{15}$$

Indeed, (15) follows directly from (14). On the other hand, since $\mathrm{Q}_{\mathrm{ali},\mathbb{M}} \geq 1$, (15) implies $\mathrm{Q}_{\mathrm{eq},\mathbb{M}}(K) \leq 1$ for all K. The latter is only possible if $\mathrm{Q}_{\mathrm{eq},\mathbb{M}}(K) = 1$ for all K due to the property (9). This also means $\mathrm{Q}_{\mathrm{ali},\mathbb{M}}(K) = 1$ for all K. Thus, (15) implies (14).

It is worth mentioning that an $\mathbb{M}$-uniform mesh satisfies

$$(F_K')^{-1}\mathbb{M}_K^{-1}(F_K')^{-T} = h_{\mathbb{M}}^{-2} I, \quad \forall K \in \mathcal{T}_h. \tag{16}$$

This is because (14) implies that all eigenvalues of $(F_K')^{-1}\mathbb{M}_K^{-1}(F_K')^{-T}$ are equal to $h_{\mathbb{M}}$.

When a mesh is far from being $\mathbb{M}$-uniform, on the other hand, we have

$$\mathrm{Q}_{\mathrm{ali},\mathbb{M}}(K) \gg 1 \quad \text{and/or} \quad \max_K \mathrm{Q}_{\mathrm{eq},\mathbb{M}}(K) \gg 1$$

and, from (9) and (13),

$$\max_K \mathrm{Q}_{\mathbb{M}}(K) \gg 1.$$

2.2 Preliminary results

In this subsection we present a few properties of the mass matrix M and the stiffness matrix A of linear finite elements, which will be used repeatedly in our analysis. Throughout the paper the less-than-or-equal sign between matrix terms means that the difference between the right-hand side and left-hand side terms is positive semidefinite.

Lemma 2.1 ([KHX, Sect. 3])**.** *The linear finite element mass matrix M and its diagonal part M_D satisfy*

$$\frac{1}{2}M_D \leq M \leq \frac{d+2}{2}M_D \quad \textit{and} \quad M_{ii} = \frac{2|\omega_i|}{(d+1)(d+2)}, \quad i = 1, \ldots, N_{vi}. \tag{17}$$

Lemma 2.2. *Let M_{lump} be the lumped linear finite element mass matrix defined through*

$$M_{ii,lump} = \int_\Omega \phi_i(\boldsymbol{x}) \cdot \sum_{j=1}^{N_{vi}} \phi_j(\boldsymbol{x})\, d\boldsymbol{x}, \quad i = 1, \ldots, N_{vi}.$$

Then

$$\frac{2|\omega_i|}{(d+1)(d+2)} \leq M_{ii,lump} \leq \frac{|\omega_i|}{d+1}. \tag{18}$$

Proof. Since

$$\phi_i(\boldsymbol{x}) \leq \sum_{j=1}^{N_{vi}} \phi_j(\boldsymbol{x}) \leq 1,$$

we have

$$M_{ii,lump} \leq \int_\Omega \phi_i(\boldsymbol{x}) \cdot 1\, d\boldsymbol{x} = \sum_{K\in\omega_i} \int_K \phi_i(\boldsymbol{x})\, d\boldsymbol{x} = \sum_{K\in\omega_i} \frac{|K|}{d+1} = \frac{|\omega_i|}{d+1}$$

and

$$M_{ii,lump} \geq \int_\Omega \phi_i(\boldsymbol{x}) \cdot \phi_i(\boldsymbol{x})\, d\boldsymbol{x} = \sum_{K\in\omega_i} \int_K \phi_i^2(\boldsymbol{x})\, d\boldsymbol{x} = \sum_{K\in\omega_i} \frac{2|K|}{(d+1)(d+2)} = \frac{2|\omega_i|}{(d+1)(d+2)}. \quad \square$$

Lemma 2.3. *The linear finite element mass matrix M and lumped mass matrix M_{lump} satisfy*

$$\frac{1}{d+2}M_{lump} \le M \le \frac{d+2}{2}M_{lump}.$$

Proof. Since $M_D \le M_{lump}$ we get the upper bound directly from (17). Combining the lower bound in (17) with the upper bound in (18) gives

$$\frac{1}{d+2}M_{lump} \le \frac{1}{(d+2)(d+1)}\,\mathrm{diag}\,(|\omega_1|,\ldots,|\omega_{N_{vi}}|) = \frac{1}{2}M_D \le M. \qquad \square$$

Lemma 2.4 ([KHX, Sect. 4])**.** *The linear finite element stiffness matrix A and its diagonal part A_D satisfy*

$$A \le (d+1)A_D. \tag{19}$$

Lemma 2.5. *Let $\mathbb{D}_K$ be the average of the diffusion matrix $\mathbb{D}$ over K,*

$$\mathbb{D}_K = \frac{1}{|K|}\int_K \mathbb{D}(\boldsymbol{x})\,d\boldsymbol{x}.$$

Then the diagonal entries of the linear finite element stiffness matrix A are bounded by

$$C_{\hat{\nabla}}\sum_{K\in\omega_i}|K|\cdot\lambda_{\min}((F_K')^{-1}\mathbb{D}_K(F_K')^{-T}) \;\le\; A_{ii} \;\le\; C_{\hat{\nabla}}\sum_{K\in\omega_i}|K|\cdot\lambda_{\max}((F_K')^{-1}\mathbb{D}_K(F_K')^{-T}), \tag{20}$$

where

$$C_{\hat{\nabla}} = \frac{d}{d+1}\left(\frac{\sqrt{d+1}}{d!}\right)^{\frac{2}{d}}. \tag{21}$$

Proof. From (6) we have

$$A_{ii} = \int_\Omega \nabla\phi_i^T\mathbb{D}\nabla\phi_i\,d\boldsymbol{x} = \sum_{K\in\omega_i}\int_K \nabla\phi_i^T\mathbb{D}\nabla\phi_i\,d\boldsymbol{x} = \sum_{K\in\omega_i}|K|\;\nabla\phi_i^T\mathbb{D}_K\nabla\phi_i.$$

Denote the gradient operator in $\hat{K}$ by $\hat{\nabla} = \partial/\partial\boldsymbol{\xi}$. By the chain rule, we have $\nabla = (F_K')^{-T}\hat{\nabla}$. Thus,

$$\begin{aligned} A_{ii} &= \sum_{K\in\omega_i}|K|\;\hat{\nabla}\hat{\phi}_i^T(F_K')^{-1}\mathbb{D}_K(F_K')^{-T}\hat{\nabla}\hat{\phi}_i \\ &\le \sum_{K\in\omega_i}|K|\;\hat{\nabla}\hat{\phi}_i^T\hat{\nabla}\hat{\phi}_i\lambda_{\max}((F_K')^{-1}\mathbb{D}_K(F_K')^{-T}). \end{aligned} \tag{22}$$

Recall that $\hat{K}$ is taken to be equilateral. Thus, we have $\hat{\nabla}\hat{\phi}_i^T\hat{\nabla}\hat{\phi}_i = C_{\hat{\nabla}}$ for all $i = 1,\ldots,d+1$. Consequently, we get

$$A_{ii} \le C_{\hat{\nabla}}\sum_{K\in\omega_i}|K|\;\lambda_{\max}((F_K')^{-1}\mathbb{D}_K(F_K')^{-T}).$$

Similarly, we can obtain the left inequality of (20). $\square$

Remark 2.1. From (13) (with $\mathbb{M}$ being replaced by $\mathbb{D}^{-1}$), the bound (20) on A_{ii} can be expressed in terms of the element quality measure $\mathrm{Q}_{\mathbb{D}^{-1}}(K)$ as

$$A_{ii} \le C_{\hat{\nabla}}h_{\mathbb{D}^{-1}}^{-2}\sum_{K\in\omega_i}|K|\,\mathrm{Q}_{\mathbb{D}^{-1}}(K). \tag{23}$$

Remark 2.2 ($\mathbb{D}^{-1}$-nonobtuse meshes). Note that Lemma 2.4 is very general and valid for any given mesh. It implies that

$$\lambda_{\max}(A) \leq (d+1) \max_i A_{ii}. \tag{24}$$

This bound can be sharpened for some special types of mesh. For example, if a mesh has no obtuse angles with respect to $\mathbb{D}^{-1}$ then A is an M-matrix (its off-diagonal entries are non-positive) and $\sum_j A_{ij} \geq 0$ for all i (e.g., see the proof of Theorem 2.1 of [LH10]). From the Gershgorin circle theorem we have

$$\lambda_{\max}(A) \leq \max_i \left(A_{ii} + \sum_{j \neq i} |A_{ij}| \right) = \max_i \left(A_{ii} - \sum_{j \neq i} A_{ij} \right) = \max_i \left(2A_{ii} - \sum_j A_{ij} \right)$$

and thus

$$\lambda_{\max}(A) \leq 2 \max_i A_{ii}. \tag{25}$$

If further the mesh is $\mathbb{D}^{-1}$-uniform, from (15) and (23) we have

$$\lambda_{\max}(A) \leq 2 \max_i A_{ii} \leq 2 C_{\hat{\nabla}} h_{\mathbb{D}^{-1}}^{-2} \max_i \sum_{K \in \omega_i} |K| \, \mathrm{Q}_{\mathbb{D}^{-1}}(K) = 2 C_{\hat{\nabla}} h_{\mathbb{D}^{-1}}^{-2} \max_i |\omega_i|. \tag{26}$$

3 Explicit time stepping and the stability condition

In this section we study stability conditions for explicit Runge-Kutta (RK) methods applied to the finite element system (5) and obtain estimates for the maximum time step.

Suppose we are given a constant time step τ. Then an explicit RK scheme with s stages of order p computes approximations $\boldsymbol{U}_n \approx \boldsymbol{U}(n\tau)$ from

$$\boldsymbol{U}_n = R(-\tau M^{-1} A) \boldsymbol{U}_{n-1} \,, \tag{27}$$

where the stability function $R(z)$ is a polynomial in z and satisfies

$$R(z) = 1 + z + \ldots + \frac{z^p}{p!} + \sum_{i=p+1}^{s} \alpha_i z^i = e^z + \mathcal{O}\left(z^{p+1}\right) . \tag{28}$$

Classical explicit RK methods have severe step size restrictions when solving stiff problems as (5) for $N_{vi} \gg 1$. An interesting alternative are stabilized explicit RK methods. These methods have an extended stability domain along the negative real axis and therefore allow for larger time steps than classical explicit one-step methods. The parameters $\alpha_{p+1}, \ldots, \alpha_s \in \mathbb{R}$ in (28) are chosen in such a way that $|R(z)| \leq 1$ for $z \in [-r_s, 0]$ and $r_s > 0$ as large as possible. Often used methods are the DUMKA methods, the Runge-Kutta-Chebychev methods (RKC) and the orthogonal Runge-Kutta-Chebychev methods (ROCK). A common practical choice is $p = 2$, but there exist also DUMKA and ROCK type methods of higher order [HW96].

In what follows we will first study stability estimates for the approximate solutions $\boldsymbol{U}_n$ obtained from (27), assuming that the full mass matrix M can be easily inverted at moderate cost, e.g., by using a Cholesky decomposition. We will also discuss consequences of lumping the mass matrix as a routine procedure for (linear) finite elements. Although appropriate mass lumping does not effect the overall accuracy, it is well-known that lumping the consistent mass

induces dispersion errors that can effect the quality of the numerical solution. More generally, we consider symmetric positive definite, surrogate matrices $\tilde{M}$ that satisfy

$$c_1\,\tilde{M} \le M \le c_2\,\tilde{M} \tag{29}$$

and have nearly the same complexity as the diagonal lumped mass matrix M_{lump}. Correction techniques for the dispersive effects of mass lumping and several efficient choices for $\tilde{M}$ can be found in [GP13]. Note that due to Lemma 2.3 we have $c_1 = 1/(d+2)$ and $c_2 = (d+2)/2$ for the special case $\tilde{M} = M_{lump}$.

3.1 Stability of explicit RK schemes

Our investigation of the stability is based on the following main observation: if B is a normal matrix and R is a rational function, then

$$\|R(B)\|_2 = \max_i |R(\lambda_i(B))|. \tag{30}$$

This fundamental relation is a direct consequence of the existence of a factorization $B = Q\,\mathrm{diag}(\lambda_1(B),\dots,\lambda_{N_{vi}}(B))\,Q^T$ with an unitary matrix Q.

Using the fact that the matrices $M^{-\frac{1}{2}}AM^{-\frac{1}{2}}$ and $A^{\frac{1}{2}}M^{-1}A^{\frac{1}{2}}$ are normal, we can prove the stability of the linear finite element approximation computed with an explicit RK method.

Theorem 3.1. *For a given explicit RK method with the polynomial stability function R, the linear finite element approximation u_n^h satisfies*

$$\left\|u_n^h\right\|_{L^2(\Omega)} \le \left\|u_0^h\right\|_{L^2(\Omega)} \quad \textit{and} \quad |||u_n^h|||_{H^1(\Omega)} \le |||u_0^h|||_{H^1(\Omega)},$$

if the time step τ is chosen such that

$$\max_i |R(-\tau\lambda_i(M^{-1}A))| \le 1\,.$$

Proof. Since R is a polynomial function, we have

$$R(-\tau M^{-1}A) = M^{-\frac{1}{2}}R(-\tau M^{-\frac{1}{2}}AM^{-\frac{1}{2}})M^{\frac{1}{2}} = A^{-\frac{1}{2}}R(-\tau A^{\frac{1}{2}}M^{-1}A^{\frac{1}{2}})A^{\frac{1}{2}}.$$

From this, it is easy to see that (27) can be written as

$$M^{\frac{1}{2}}\boldsymbol{U}_n = R(-\tau M^{-\frac{1}{2}}AM^{-\frac{1}{2}})M^{\frac{1}{2}}\boldsymbol{U}_{n-1}, \tag{31}$$

$$A^{\frac{1}{2}}\boldsymbol{U}_n = R(-\tau A^{\frac{1}{2}}M^{-1}A^{\frac{1}{2}})A^{\frac{1}{2}}\boldsymbol{U}_{n-1}. \tag{32}$$

Since M and A are symmetric and positive definite, $M^{-\frac{1}{2}}AM^{-\frac{1}{2}}$ and $A^{\frac{1}{2}}M^{-1}A^{\frac{1}{2}}$ are symmetric and therefore normal. From (30), our assumption on the time step and from the fact that $M^{-1}A$, $M^{-\frac{1}{2}}AM^{-\frac{1}{2}}$, and $A^{\frac{1}{2}}M^{-1}A^{\frac{1}{2}}$ are similar to each other, we get

$$\left\|R(-\tau M^{-\frac{1}{2}}AM^{-\frac{1}{2}})\right\|_2 = \left\|R(-\tau A^{\frac{1}{2}}M^{-1}A^{\frac{1}{2}})\right\|_2 = \max_i \left|R(-\tau\lambda_i(M^{-1}A))\right| \le 1.$$

Thus, equations (31) and (32) imply

$$\left\|u_n^h\right\|_{L^2(\Omega)} = \left\|M^{\frac{1}{2}}\boldsymbol{U}_n\right\|_2 \le \left\|M^{\frac{1}{2}}\boldsymbol{U}_{n-1}\right\|_2 = \left\|u_{n-1}^h\right\|_{L^2(\Omega)}$$

and

$$|||u_n^h|||_{H^1(\Omega)} = \left\|A^{\frac{1}{2}}\boldsymbol{U}_n\right\|_2 \le \left\|A^{\frac{1}{2}}\boldsymbol{U}_{n-1}\right\|_2 = |||u_{n-1}^h|||_{H^1(\Omega)}.$$

Successive application of these inequalities yields the assertion. □

We next consider the case where the linear finite element mass matrix M is replaced by a symmetric positive definite, surrogate matrix $\tilde{M}$ of lower complexity. That means, from now on we compute approximations $\boldsymbol{U}_n \approx \boldsymbol{U}(n\tau)$ from

$$\boldsymbol{U}_n = R(-\tau\, \tilde{M}^{-1}A)\boldsymbol{U}_{n-1}\,. \tag{33}$$

Theorem 3.2. *For a given explicit RK method with the polynomial stability function R and a symmetric positive definite, surrogate matrix $\tilde{M}$ that satisfies $c_1\tilde{M} \le M \le c_2\tilde{M}$ for some positive constants c_1 and c_2, the linear finite element approximation u_n^h satisfies*

$$\left\|u_n^h\right\|_{L^2(\Omega)} \le \sqrt{\frac{c_2}{c_1}}\left\|u_0^h\right\|_{L^2(\Omega)} \quad \textit{and} \quad |||u_n^h|||_{H^1(\Omega)} \le |||u_0^h|||_{H^1(\Omega)},$$

if the time step τ is chosen such that

$$\max_i |R(-\tau\lambda_i(\tilde{M}^{-1}A))| \le 1\,.$$

Proof. Replacing M by $\tilde{M}$ in the proof of Theorem 3.1 does not change the arguments and gives

$$|||u_n^h|||_{H^1(\Omega)} = \left\|A^{\frac{1}{2}}\boldsymbol{U}_n\right\|_2 \le \left\|A^{\frac{1}{2}}\boldsymbol{U}_{n-1}\right\|_2 = |||u_{n-1}^h|||_{H^1(\Omega)}$$

and

$$\left\|\tilde{M}^{\frac{1}{2}}\boldsymbol{U}_n\right\|_2 \le \left\|\tilde{M}^{\frac{1}{2}}\boldsymbol{U}_{n-1}\right\|_2.$$

From the first inequality, stability in the energy norm follows. To derive stability in the L^2-norm, we make use of the assumption on $\tilde{M}$:

$$\begin{aligned}
\left\|u_n^h\right\|_{L^2(\Omega)}^2 &= (\boldsymbol{U}_n)^T M\boldsymbol{U}_n \\
&\le c_2\,(\boldsymbol{U}_n)^T\tilde{M}\boldsymbol{U}_n = c_2\left\|\tilde{M}^{\frac{1}{2}}\boldsymbol{U}_n\right\|_2 \\
&\le c_2\left\|\tilde{M}^{\frac{1}{2}}\boldsymbol{U}_{n-1}\right\|_2 \le \cdots \\
&\le c_2\left\|\tilde{M}^{\frac{1}{2}}\boldsymbol{U}_0\right\|_2 = c_2\,(\boldsymbol{U}_0)^T\tilde{M}\boldsymbol{U}_0 \\
&\le \frac{c_2}{c_1}\,(\boldsymbol{U}_0)^T M\boldsymbol{U}_0 = \frac{c_2}{c_1}\left\|u_0^h\right\|_{L^2(\Omega)}^2,
\end{aligned}$$

which gives the desired result. □

In the special case $\tilde{M} = M_{lump}$ we have the following result.

Corollary 3.2.1. *Under the assumptions of Theorem 3.2 and $\tilde{M} = M_{lump}$, we have*

$$\left\|u_n^h\right\|_{L^2(\Omega)} \le \frac{d+2}{\sqrt{2}}\left\|u_0^h\right\|_{L^2(\Omega)} \quad \textit{and} \quad |||u_n^h|||_{H^1(\Omega)} \le |||u_0^h|||_{H^1(\Omega)}\,.$$

3.2 Estimates on the largest eigenvalue of $\tilde{M}^{-1}A$

The above results show that the contractivity of any given explicit Runge-Kutta method is guaranteed if all eigenvalues of $-\tau\tilde{M}^{-1}A$ are in the corresponding stability domain $\mathcal{S} = \{z \in \mathbb{C} : |R(z)| \leq 1\}$. As a consequence, the key to the stability analysis of a given scheme is to estimate the eigenvalues of $\tilde{M}^{-1}A$. The following theorem provides such an estimate for two choices of $\tilde{M}$: $\tilde{M} = M$ and $\tilde{M} = M_{lump}$. It turns out that in these cases the largest eigenvalue of $\tilde{M}^{-1}A$ is equivalent to the largest ratio between the corresponding diagonal entries of A and $\tilde{M}$.

Theorem 3.3. *The eigenvalues of $\tilde{M}^{-1}A$ with $\tilde{M}$ being either M or M_{lump} are real and positive. Moreover, the largest eigenvalue is bounded by*

$$\max_i \frac{A_{ii}}{\tilde{M}_{ii}} \leq \lambda_{\max}(\tilde{M}^{-1}A) \leq C_* \max_i \frac{A_{ii}}{\tilde{M}_{ii}}, \tag{34}$$

where C_* is given in Table 1.

Table 1: C_* in Theorem 3.3

	general meshes	nonobtuse meshes w.r.t. $\mathbb{D}^{-1}$
$\tilde{M} = M$	$2(d+1)$	4
$\tilde{M} = M_{lump}$	$d+1$	2

Proof. Since $\tilde{M}$ and A are symmetric and positive definite and since $\tilde{M}^{-1}A$ is similar to the symmetric matrix $\tilde{M}^{-\frac{1}{2}}A\tilde{M}^{-\frac{1}{2}}$, the eigenvalues of $\tilde{M}^{-1}A$ are real and positive.

Using the canonical basis vectors $\boldsymbol{e}_i$ gives

$$\lambda_{\max}(\tilde{M}^{-1}A) = \max_{\boldsymbol{v}\neq 0} \frac{\boldsymbol{v}^T A\boldsymbol{v}}{\boldsymbol{v}^T\tilde{M}\boldsymbol{v}} \geq \max_i \frac{\boldsymbol{e}_i^T A\boldsymbol{e}_i}{\boldsymbol{e}_i^T\tilde{M}\boldsymbol{e}_i} = \max_i \frac{A_{ii}}{\tilde{M}_{ii}}.$$

Let us first have a look at the case $\tilde{M} = M$. Lemmas 2.1 and 2.4 yield

$$\begin{aligned} \lambda_{\max}(M^{-1}A) &= \max_{\boldsymbol{v}\neq 0} \frac{\boldsymbol{v}^T A\boldsymbol{v}}{\boldsymbol{v}^T M\boldsymbol{v}} \\ &\leq \max_{\boldsymbol{v}\neq 0} \frac{(d+1)\boldsymbol{v}^T A_D\boldsymbol{v}}{\frac{1}{2}\boldsymbol{v}^T M_D\boldsymbol{v}} \\ &= 2(d+1)\max_i \frac{A_{ii}}{M_{ii}}. \end{aligned} \tag{35}$$

For the special case of meshes with nonobtuse angles with respect to $\mathbb{D}^{-1}$, the above bound can be sharpened by replacing the factor $d+1$ in (35) with 2 (cf. Remark 2.2). Moreover, if $\tilde{M} = M_{lump}$, the factor $1/2$ in the denominator of (35) can be replaced by 1 since M_{lump} is already diagonal. □

Example 3.1 (Stabilized Runge-Kutta methods). The stability region of a stabilized RK method of order $p = 1$ with s stages extends along the negative real axis of the complex plane, including

the interval $[-2s^2, 0]$ [HW96, p. 31f.]. Thus, the method is stable if all eigenvalues of $-\tau\tilde{M}^{-1}A$ are between $-2s^2$ and 0. This leads to the stability condition

$$\tau \leq \frac{2s^2}{\lambda_{\max}(\tilde{M}^{-1}A)}. \tag{36}$$

Using Theorem 3.3 and noticing $\max_i \frac{A_{ii}}{\tilde{M}_{ii}} = \min_i \frac{\tilde{M}_{ii}}{A_{ii}}$, we obtain a bound for the largest permissible time step $\tau_{\max}$ as

$$\frac{2s^2}{C_*} \min_i \frac{\tilde{M}_{ii}}{A_{ii}} \leq \tau_{\max} \leq 2s^2 \min_i \frac{\tilde{M}_{ii}}{A_{ii}}. \tag{37}$$

Clearly, if

$$\tau > 2s^2 \min_i \frac{\tilde{M}_{ii}}{A_{ii}},$$

we have $\left|R(-\tau\lambda_{\max}(\tilde{M}^{-1}A))\right| > 1$ and the scheme becomes unstable. In order to guarantee stability, the step size has to be chosen such that

$$\tau \leq \frac{2s^2}{C_*} \min_i \frac{\tilde{M}_{ii}}{A_{ii}}.$$

Note that here $\tilde{M} = M$ or $\tilde{M} = M_{lump}$.

The estimate in Theorem 3.3 is easy to use in actual computation. However, it does not reveal how the mesh geometry comes into play. To investigate this, we provide an upper bound on $\lambda_{\max}(\tilde{M}^{-1}A)$ in terms of the mesh quality measures.

Corollary 3.3.1. *The largest eigenvalue of $\tilde{M}^{-1}A$ is bounded by*

$$\lambda_{\max}(\tilde{M}^{-1}A) \leq \frac{C_* C_{\hat{\nabla}}(d+1)(d+2)}{2h^2_{\mathbb{D}^{-1}}} \max_i \frac{1}{|\omega_i|} \sum_{K\in\omega_i} |K|\ \mathrm{Q}_{\mathbb{D}^{-1}}(K) \tag{38}$$

$$= \frac{C_* C_{\hat{\nabla}}(d+1)(d+2)}{2} \max_i \frac{1}{|\omega_i|} \sum_{K\in\omega_i} |K| \cdot \left\|(F'_K)^{-1}\mathbb{D}_K(F'_K)^{-T}\right\|_2, \tag{39}$$

where constants $C_{\hat{\nabla}}$ and C_* are given in (21) and Table 1, respectively, and the element quality $\mathrm{Q}_{\mathbb{D}^{-1}}(K)$ is defined in (13) (with $\mathbb{M}$ being replaced by $\mathbb{D}^{-1}$).

Proof. The bound can be obtained by substituting (17) and (23) for $\tilde{M}_{ii}$ and A_{ii} in Theorem 3.3. □

The factor $h^{-2}_{\mathbb{D}^{-1}}$ in (38) corresponds to h^2 in the classic stability condition $\tau \sim h^2$ for uniform meshes with the Laplace operator. Since

$$h_{\mathbb{D}^{-1}} = (|\Omega|_{\mathbb{D}^{-1},h}/N)^{\frac{1}{d}} \to (|\Omega|_{\mathbb{D}^{-1}}/N)^{\frac{1}{d}}$$

as the mesh is being refined, $h_{\mathbb{D}^{-1}}$ can be considered independent of the mesh geometry (and therefore it essentially depends only on N, $\mathbb{D}^{-1}$, and Ω). The effect of the mesh geometry is reflected mainly through the patch-average of the element quality measure $\mathrm{Q}_{\mathbb{D}^{-1}}(K)$. Hence, we can conclude that the largest possible time step $\tau_{\max}$ depends on *the number of mesh elements*

and on *how far the mesh is from being uniform with respect to* $\mathbb{D}^{-1}$. In particular, *it is not the mesh geometry itself but the mesh geometry in relation to the diffusion matrix that matters for the stability of explicit schemes.*

We now study the situation with an $\mathbb{M}$-uniform mesh for a general metric tensor $\mathbb{M}$. Recall that such a mesh satisfies (16), which can be rewritten as

$$(F_K')^{-T}(F_K')^{-1} = h_{\mathbb{M}}^{-2}\mathbb{M}_K, \quad \forall K \in \mathcal{T}_h.$$

Then,

$$\mathrm{Q}_{\mathbb{D}^{-1}}(K) = h_{\mathbb{D}^{-1}}^2 \left\| (F_K')^{-1}\mathbb{D}_K(F_K')^{-T} \right\|_2 = h_{\mathbb{D}^{-1}}^2 \left\| (F_K')^{-T}(F_K')^{-1}\mathbb{D}_K \right\|_2 = \left(\frac{h_{\mathbb{D}^{-1}}}{h_{\mathbb{M}}}\right)^2 \|\mathbb{M}_K\mathbb{D}_K\|_2.$$

Inserting this into (38), we get

$$\lambda_{\max}(\tilde{M}^{-1}A) \le \frac{C_* C_{\hat{\nabla}}(d+1)(d+2)}{2h_{\mathbb{M}}^2} \max_i \frac{1}{|\omega_i|} \sum_{K\in\omega_i} |K| \cdot \|\mathbb{M}_K\mathbb{D}_K\|_2. \tag{40}$$

Once again, this shows that the largest eigenvalue of $\tilde{M}^{-1}A$ and, consequently, the largest permissible time step depend on the number of elements and the matching between the mesh (essentially determined by $\mathbb{M}$) and the diffusion matrix.

Remark 3.1 (Coefficient-adaptive meshes). For meshes with $\mathbb{M} = \mathbb{D}^{-1}$, i.e., coefficient-adaptive ($\mathbb{D}^{-1}$-uniform) meshes, from (16) (with $\mathbb{M} = \mathbb{D}^{-1}$) and (22) we have

$$A_{ii} = \frac{C_{\hat{\nabla}}|\omega_i|}{h_{\mathbb{D}^{-1}}^2}.$$

This, together with (17) and Theorem 3.3, yields

$$\frac{C_{\hat{\nabla}}(d+1)(d+2)}{2h_{\mathbb{D}^{-1}}^2} \le \lambda_{\max}(\tilde{M}^{-1}A) \le \frac{C_* C_{\hat{\nabla}}(d+1)(d+2)}{2h_{\mathbb{D}^{-1}}^2}. \tag{41}$$

The bound is tight within a factor of C_*.

Remark 3.2 (Comparison to results available in the literature). Corollary 3.3.1 is similar to the result by Zhu and Du [ZD14, Theorem 3.1]. In the current notation, their estimate can be written as

$$\begin{aligned}\frac{4C_0 \max_K \lambda_{\min}(\mathbb{D}_K)\left\|(F_K')^{-1}(F_K')^{-T}\right\|_2}{(d-1)(2+(d+2)c_1 p_{\max})} &\le \lambda_{\max}(M^{-1}A) \\ &\le C_0(d+2)\max_K \lambda_{\max}(\mathbb{D}_K)\left\|(F_K')^{-1}(F_K')^{-T}\right\|_2,\end{aligned} \tag{42}$$

where C_0 is a (explicitly computable) mesh-independent constant, $p_{\max}$ is the maximum number of elements in a patch, and c_1 is the maximum ratio of volumes of neighboring elements.

However, there are significant differences between Corollary 3.3.1 and (42). The effects of the interplay between the mesh geometry and the diffusion matrix on the time step in (39) and (42) are reflected by the factors

$$\max_i \frac{1}{|\omega_i|}\sum_{K\in\omega_i} |K| \cdot \left\|(F_K')^{-1}\mathbb{D}_K(F_K')^{-T}\right\|_2 \quad \text{and} \quad \max_K \lambda_{\max}(\mathbb{D}_K)\left\|(F_K')^{-1}(F_K')^{-T}\right\|_2,$$

respectively. Note that the former is smaller than the latter. As we have seen in Sect. 2.1, $\left\|(F'_K)^{-1}\mathbb{D}_K(F'_K)^{-T}\right\|_2$, which is proportional to the element quality measure $\mathrm{Q}_{\mathbb{D}^{-1}}(K)$, indicates how far K is from being unitary (in volume) and equilateral in the metric specified by $\mathbb{D}_K^{-1}$ and provides a proper, accurate measure for the interplay between the mesh geometry and $\mathbb{D}$. On the other hand, $\lambda_{\max}(\mathbb{D}_K)\left\|(F'_K)^{-1}(F'_K)^{-T}\right\|_2$ does not take into consideration the alignment of the shape and orientation of K with $\mathbb{D}$ and therefore is not an accurate measure for the interplay (see Example 4.4 for a numerical example). Note that for an anisotropic $\mathbb{D}$ the accuracy of (42) deteriorates proportionally to $\kappa(\mathbb{D})$.

Moreover, our bound in terms of matrix entries (Theorem 3.3) is sharp within a constant which is completely independent of the mesh and the diffusion matrix. The ratio of the upper bound to the lower one is at most

$$2(d+1),$$

whereas this ratio for (42) is approximately

$$d(d+2)^2\kappa(\mathbb{D})c_1 p_{\max}.$$

For an isotropic diffusion and a locally quasi-uniform 2D mesh ($\kappa(\mathbb{D}) = 1$, $d = 2$, $p_{\max} \approx 6$, $c_1 \approx 1$) we have $(d+2)^2\kappa(\mathbb{D})c_1 p_{\max} = 2 \cdot 4^2 \cdot 1 \cdot 1 \cdot 6 = 192$. If we assume that the lower and upper bounds are equally tight, than (42) would underestimate the exact value of $\lambda_{\max}$ and, thus, that of $\tau_{\max}$ by a factor of $\sqrt{192} \approx 13.86$, which is consistent with the numerical results [ZD11; ZD14] showing a range of 12.00 to 19.48. In comparison, the estimate (34) would underestimate the exact value of $\tau_{\max}$ by a factor of approximately $\sqrt{2(d+1)} = \sqrt{6} \approx 2.45$, which is in a good agreement with numerical results of (Examples 4.2 and 4.3) showing a range of 1.14 to 3.87.

4 Numerical examples

To test the developed estimates we continue Example 3.1 (stabilized Runge-Kutte methods) and compare the exact value of the largest permissible time step (36)

$$\tau_{\max} = \frac{2s^2}{\lambda_{\max}(M^{-1}A)},$$

with the lower bound (37)

$$\tau_h = \frac{2s^2}{C_*}\min_i \frac{M_{ii}}{A_{ii}},$$

and compute the ratio $\tau_{\max}/\tau_h$ to evaluate the accuracy of the estimate. Since $\tau_{\max}/\tau_h$ is independent of the number of stages s, we rescale the values of $\tau_{\max}$ and τ_h by s^{-2} to stay general, i.e., in the following we compare

$$\frac{\tau_{\max}}{s^2} = \frac{2}{\lambda_{\max}(M^{-1}A)} \qquad \text{with} \qquad \frac{\tau_h}{s^2} = \frac{2}{C_*}\min_i \frac{M_{ii}}{A_{ii}}.$$

Note that (37) implies that $1 \le \tau_{\max}/\tau_h \le C_*$ for any mesh and any diffusion matrix $\mathbb{D}$. Moreover, from (40),

$$\frac{\tau_{\max}}{s^2} \ge \frac{4h_{\mathbb{M}}^2}{C_* C_{\hat{\nabla}}(d+1)(d+2)\max_i \frac{1}{|\omega_i|}\sum\limits_{K\in\omega_i}|K|\cdot\|\mathbb{M}_K\mathbb{D}_K\|_2}. \tag{43}$$

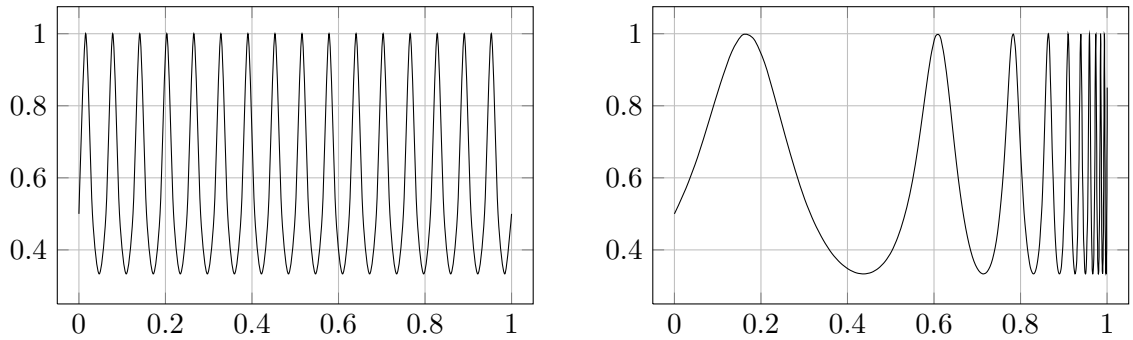

(a) periodic (b) nonperiodic

Figure 2: Diffusion coefficient $\mathbb{D}$ (Example 4.1).

Example 4.1 (1D example [PS12, Sects. 6.1 and 6.2]). As a first example we consider the heat diffusion

$$u_t = \mathbb{D} \cdot u_{xx} \quad \text{in } \Omega = (0,1)$$

with the periodic (Fig. 2a) and nonperiodic (Fig. 2b) diffusion coefficients

$$\mathbb{D}(x) = \left(2 - \sin\left(2\pi \frac{x}{\varepsilon}\right)\right)^{-1}, \qquad \mathbb{D}(x) = \left(2 - \sin\left(2\pi \tan \frac{(1-\varepsilon)\pi x}{2}\right)\right)^{-1},$$

where ε is a positive parameter. We choose $\varepsilon = 2^{-4}$ for our tests.

Numerical results in Table 2 show that $1.00 \le \tau_{\max}/\tau_h \le 1.45$ for all considered meshes and cases, which is consistent with the theoretical prediction $1 \le \tau_{\max}/\tau_h \le 2$ (with mass lumping) and $1 \le \tau_{\max}/\tau_h \le 4$ (no mass lumping). Interestingly, for this example, the estimate appears to be even asymptotically exact ($\tau_{\max}/\tau_h \to 1$ as $N \to \infty$) except for the case of $\mathbb{D}^{-1}$-uniform meshes with mass lumping.

Table 2 further shows that $\tau_{\max}$ in case of mass lumping is roughly three times as large as $\tau_{\max}$ without mass lumping. The largest permissible time step $\tau_{\max}$ for $\mathbb{D}^{-1}$-uniform meshes (Tables 2c and 2d) is approximately 1.4 to 1.8 times as large as for uniform meshes (Tables 2a and 2b).

Example 4.2 (2D example, $\mathbb{D} = I$). In this example we consider the simplest case of $\mathbb{D} = I$. Mesh examples are taken from [ZD11; ZD14]; they are: uniform isotropic, uniform anisotropic and strongly refined towards the boundary. Since these meshes have no obtuse angles, we can use sharper bounds with $C_* = 2$ (mass lumping) or $C_* = 4$ (no mass lumping) and therefore we expect that $1 \le \tau_{\max}/\tau_h \le 2$ or $1 \le \tau_{\max}/\tau_h \le 4$, respectively.

Table 3 shows that $1.14 \le \tau_{\max}/\tau_h \le 1.69$ (mass lumping) and $1.18 \le \tau_{\max}/\tau_h \le 2.33$ (no mass lumping). In comparison, the same ratio for numerical examples in [ZD11; ZD14] ranges from 12.00 to 19.48. This difference is partially due to the fact that estimates in terms of mesh geometry are generally less tight than those in terms of matrix entries since additional estimation steps decrease the accuracy. Nevertheless, the new estimate (38) (or (43)) in terms of mesh geometry is more accurate than those in [ZD11; ZD14]. Consider the case with $\mathbb{D} = I$. The estimate [ZD14, Eq. 6.1] yields for the explicit Euler scheme with uniform meshes (Fig. 3a)

$$\tau_{\max} \ge \frac{1}{24N}$$

Table 2: Numerical results in 1D (Example 4.1)

(a) periodic $\mathbb{D}$, uniform meshes

	with mass lumping			without mass lumping		
N	$\tau_{\max}/s^2$	τ_h/s^2	$\tau_{\max}/\tau_h$	$\tau_{\max}/s^2$	τ_h/s^2	$\tau_{\max}/\tau_h$
64	1.84×10^{-4}	1.27×10^{-4}	1.45	6.57×10^{-5}	5.10×10^{-5}	1.29
128	3.79×10^{-5}	3.26×10^{-5}	1.16	1.45×10^{-5}	1.09×10^{-5}	1.32
256	8.66×10^{-6}	7.76×10^{-6}	1.12	3.11×10^{-6}	2.59×10^{-6}	1.20
512	2.04×10^{-6}	1.91×10^{-6}	1.06	7.08×10^{-7}	6.37×10^{-7}	1.11
1 024	4.93×10^{-7}	4.77×10^{-7}	1.03	1.68×10^{-7}	1.59×10^{-7}	1.06
2 048	1.21×10^{-7}	1.19×10^{-7}	1.02	4.09×10^{-8}	3.97×10^{-8}	1.03

(b) nonperiodic $\mathbb{D}$, uniform meshes

	with mass lumping			without mass lumping		
N	$\tau_{\max}/s^2$	τ_h/s^2	$\tau_{\max}/\tau_h$	$\tau_{\max}/s^2$	τ_h/s^2	$\tau_{\max}/\tau_h$
64	1.25×10^{-4}	1.19×10^{-4}	1.05	4.31×10^{-5}	3.96×10^{-5}	1.09
128	3.09×10^{-5}	3.01×10^{-5}	1.03	1.05×10^{-5}	1.00×10^{-5}	1.04
256	7.67×10^{-6}	7.57×10^{-6}	1.01	2.58×10^{-6}	2.52×10^{-6}	1.02
512	1.91×10^{-6}	1.90×10^{-6}	1.01	6.41×10^{-7}	6.33×10^{-7}	1.01
1 024	4.78×10^{-7}	4.76×10^{-7}	1.00	1.60×10^{-7}	1.59×10^{-7}	1.01
2 048	1.19×10^{-7}	1.19×10^{-7}	1.00	3.98×10^{-8}	3.97×10^{-8}	1.00

(c) periodic $\mathbb{D}$, $\mathbb{D}^{-1}$-uniform meshes

	with mass lumping			without mass lumping		
N	$\tau_{\max}/s^2$	τ_h/s^2	$\tau_{\max}/\tau_h$	$\tau_{\max}/s^2$	τ_h/s^2	$\tau_{\max}/\tau_h$
64	2.30×10^{-4}	1.86×10^{-4}	1.23	7.67×10^{-5}	7.54×10^{-5}	1.02
128	5.86×10^{-5}	4.86×10^{-5}	1.21	1.96×10^{-5}	1.94×10^{-5}	1.01
256	1.47×10^{-5}	1.22×10^{-5}	1.21	4.91×10^{-6}	4.90×10^{-6}	1.00
512	3.69×10^{-6}	3.06×10^{-6}	1.21	1.23×10^{-6}	1.23×10^{-6}	1.00
1 024	9.22×10^{-7}	7.67×10^{-7}	1.20	3.07×10^{-7}	3.07×10^{-7}	1.00
2 048	2.31×10^{-7}	1.92×10^{-7}	1.20	7.68×10^{-8}	7.68×10^{-8}	1.00

(d) nonperiodic $\mathbb{D}$, $\mathbb{D}^{-1}$-uniform meshes

	with mass lumping			without mass lumping		
N	$\tau_{\max}/s^2$	τ_h/s^2	$\tau_{\max}/\tau_h$	$\tau_{\max}/s^2$	τ_h/s^2	$\tau_{\max}/\tau_h$
64	2.04×10^{-4}	1.68×10^{-4}	1.22	7.09×10^{-5}	6.59×10^{-5}	1.08
128	5.28×10^{-5}	4.18×10^{-5}	1.26	1.82×10^{-5}	1.67×10^{-5}	1.09
256	1.32×10^{-5}	1.10×10^{-5}	1.21	4.53×10^{-6}	4.24×10^{-6}	1.07
512	3.43×10^{-6}	2.76×10^{-6}	1.25	1.15×10^{-6}	1.12×10^{-6}	1.02
1 024	8.65×10^{-7}	6.98×10^{-7}	1.24	2.89×10^{-7}	2.86×10^{-7}	1.01
2 048	2.17×10^{-7}	1.77×10^{-7}	1.22	7.23×10^{-8}	7.20×10^{-8}	1.00

whereas (43) gives

$$\tau_{\max} \geq \frac{1}{12N}.$$

Notice the significant reduction of $\tau_{\max}$ when the mesh gets adapted in the "wrong" way (away from $\mathbb{D}^{-1}$). For example, a 32×32 uniform mesh requires $\tau_{\max} = 2.38{\times}10^{-4}$, whereas the 4×256 mesh with the same number of elements requires $\tau_{\max} = 6.36{\times}10^{-6}$, a reduction by a factor of 37 (Table 3b). A strongly anisotropic mesh adapted towards the boundary with a much smaller number of elements (4×16, Table 3c) leads to the further reduction of the step size by a factor of 3 000. Thus, the matching between the element geometry and the diffusion matrix has significant effects on the time step size and, depending on the anisotropy of the mesh and diffusion matrix, changes in the mesh alignment can result in changes in the time step size by orders of magnitude.

Again, mass lumping allows approximately 1.9 to 3.2 times larger time steps.

Example 4.3 (2D ground water flow with jumping coefficients [MP08]). As the next example we consider ground water flow through an aquifer. The problem is given by the IBVP (1) with $\Omega = (0, 100) \times (0, 100)$ and two impermeable subdomains $\Omega_1 = (0, 80) \times (64, 68)$ and $\Omega_2 = (20, 100) \times (40, 44)$. Figure 4 shows the diffusion coefficients and the boundary conditions. Although the diffusion matrix $\mathbb{D}$ is isotropic, it has a jump between the subdomains, leading to the anisotropic behavior of the solution.

We compute the solution by h-refinement in the standard way and use Hessian recovery based mesh adaptation to obtain adaptive meshes at particular time points and compare the exact $\tau_{\max}$ with the lower bound τ_h. For our computation we used `KARDOS` [ELR02] for solving the PDE and `BAMG` [Hec] for generating the mesh. Examples of adaptive meshes are shown in Fig. 5 for the time points $1.0{\times}10^2$, $5.0{\times}10^3$, $1.0{\times}10^4$ and $1.0{\times}10^5$.

Table 4 shows that the ratio $\tau_{\max}/\tau_h$ is about 3.25 to 3.87 without mass lumping and 2.13 to 2.48 with mass lumping, which is consistent with the theoretical upper bounds $2(d+1) = 6$ and $d + 1 = 3$.

In this example, mass lumping would allow 2.6 to 2.8 times larger time steps, which is similar to Example 4.2 (a factor of 1.9 to 3.2 there).

Example 4.4 (2D anisotropic diffusion). In this example we would like to show the importance of the interplay between the major diffusion directions and the mesh geometry. For this purpose we compare the new estimate (39) in terms of mesh geometry with the estimate (42), which represents estimates available in the literature [ZD11; ZD14].

Consider the IBVP (1) with homogeneous Dirichlet boundary condition and

$$\mathbb{D} = \begin{bmatrix} \cos\theta & -\sin\theta \\ \sin\theta & \cos\theta \end{bmatrix} \begin{bmatrix} 1000 & 0 \\ 0 & 1 \end{bmatrix} \begin{bmatrix} \cos\theta & \sin\theta \\ -\sin\theta & \cos\theta \end{bmatrix}, \quad \theta = \pi \sin x \cos y, \quad \Omega = (0,1)^2 \setminus \left[\frac{4}{9}, \frac{5}{9}\right]^2.$$

First, we consider quasi-uniform meshes (Table 5a), for which elements are close to be uniform in shape and size, $F_K' \approx |K|^{1/d} I$ and $\|(F_K')^{-1}\mathbb{D}_K(F_K')^{-T}\|_2 \approx \lambda_{\max}(\mathbb{D})\|(F_K')^{-1}(F_K')^{-T}\|_2$. Hence, bounds (39) and (42) will provide comparable results. This is confirmed by the numerical results in Table 5a, i.e., (39) and (42) are accurate within a factor of 16 to 20 and 33 to 35, respectively.

We now consider $\mathbb{D}^{-1}$-uniform (coefficient-adaptive) meshes (Table 5b). In this case the situation is quite different and, as mentioned in Remark 3.2, bound (39) will be more accurate than (42). This is confirmed by the numerical results in Table 5b: bound (39) in Corollary 3.3.1

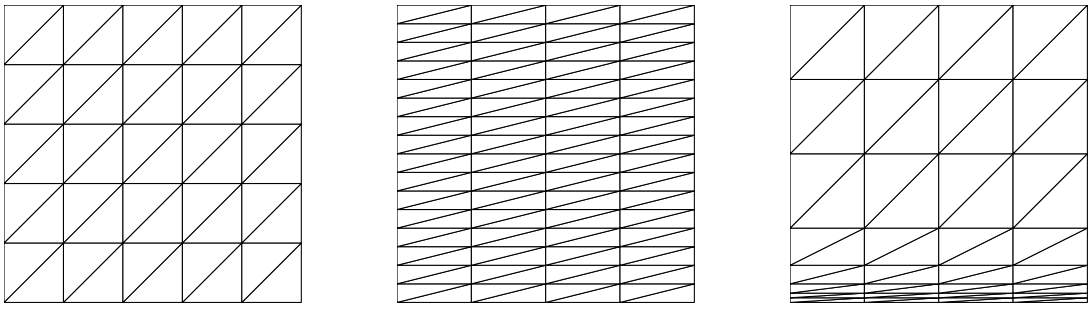

(a) uniform isotropic (b) uniform anisotropic (c) boundary layer

Figure 3: Meshes considered in Example 4.2

Table 3: Numerical results for meshes in Example 4.2

(a) uniform isotropic

		with mass lumping			without mass lumping		
mesh	N	$\tau_{\max}/s^2$	τ_h/s^2	$\tau_{\max}/\tau_h$	$\tau_{\max}/s^2$	τ_h/s^2	$\tau_{\max}/\tau_h$
8×8	128	3.79×10^{-3}	2.60×10^{-3}	1.46	1.31×10^{-3}	9.77×10^{-4}	1.34
16×16	512	9.53×10^{-4}	6.51×10^{-4}	1.46	3.09×10^{-4}	2.44×10^{-4}	1.27
32×32	2 048	2.38×10^{-4}	1.63×10^{-4}	1.46	7.60×10^{-5}	6.10×10^{-5}	1.25
64×64	8 192	5.96×10^{-5}	4.07×10^{-5}	1.46	1.89×10^{-5}	1.53×10^{-5}	1.24
128×128	32 768	1.49×10^{-5}	1.02×10^{-5}	1.46	4.72×10^{-6}	3.81×10^{-6}	1.24

(b) uniform anisotropic

		with mass lumping			without mass lumping		
mesh	N	$\tau_{\max}/s^2$	τ_h/s^2	$\tau_{\max}/\tau_h$	$\tau_{\max}/s^2$	τ_h/s^2	$\tau_{\max}/\tau_h$
32×32	2 048	2.38×10^{-4}	1.63×10^{-4}	1.46	7.60×10^{-5}	6.10×10^{-5}	1.25
16×64	2 048	9.86×10^{-5}	7.66×10^{-5}	1.29	3.40×10^{-5}	2.87×10^{-5}	1.18
8×128	2 048	2.54×10^{-5}	2.03×10^{-5}	1.25	9.00×10^{-6}	7.60×10^{-6}	1.18
4×256	2 048	6.36×10^{-6}	5.08×10^{-6}	1.25	2.38×10^{-6}	1.91×10^{-6}	1.25
2×512	2 048	1.27×10^{-6}	1.11×10^{-6}	1.14	6.36×10^{-7}	4.77×10^{-7}	1.33

(c) boundary layer

		with mass lumping			without mass lumping		
mesh	N	$\tau_{\max}/s^2$	τ_h/s^2	$\tau_{\max}/\tau_h$	$\tau_{\max}/s^2$	τ_h/s^2	$\tau_{\max}/\tau_h$
4×8	64	1.37×10^{-4}	8.11×10^{-5}	1.69	7.08×10^{-5}	3.04×10^{-5}	2.33
4×10	80	8.61×10^{-6}	5.08×10^{-6}	1.69	4.45×10^{-6}	1.91×10^{-6}	2.33
4×12	96	5.38×10^{-7}	3.18×10^{-7}	1.69	2.78×10^{-7}	1.19×10^{-7}	2.33
4×14	112	3.36×10^{-8}	1.99×10^{-8}	1.69	1.74×10^{-8}	7.45×10^{-9}	2.33
4×16	128	2.10×10^{-9}	1.24×10^{-9}	1.69	1.09×10^{-9}	4.66×10^{-10}	2.33

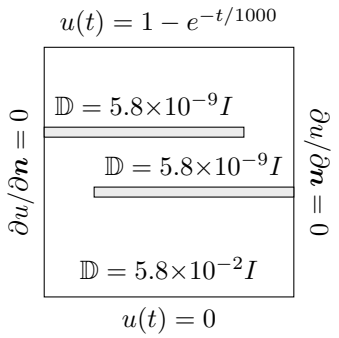

Figure 4: Domain and the diffusion $\mathbb{D}$ for the ground water flow example (Example 4.3)

Table 4: Numerical results for the ground water flow example (Example 4.3)

		with mass lumping			without mass lumping		
time	N	$\tau_{\max}/s^2$	τ_h/s^2	$\tau_{\max}/\tau_h$	$\tau_{\max}/s^2$	τ_h/s^2	$\tau_{\max}/\tau_h$
$1.0{\times}10^2$	3 071	$1.48{\times}10^0$	$5.97{\times}10^{-1}$	2.48	$5.77{\times}10^{-1}$	$1.49{\times}10^{-1}$	3.87
$5.0{\times}10^3$	2 799	$4.74{\times}10^0$	$2.23{\times}10^0$	2.13	$1.81{\times}10^0$	$5.57{\times}10^{-1}$	3.25
$1.0{\times}10^4$	5 305	$1.80{\times}10^0$	$8.01{\times}10^{-1}$	2.25	$6.89{\times}10^{-1}$	$2.00{\times}10^{-1}$	3.44
$1.0{\times}10^5$	20 334	$2.05{\times}10^{-1}$	$9.11{\times}10^{-2}$	2.25	$7.45{\times}10^{-2}$	$2.28{\times}10^{-2}$	3.27

is accurate within a factor of 8 to 11, whereas (42) underestimates the real value by a factor of 5 611 to 7 698.

This example also shows that $\mathbb{D}^{-1}$-uniform meshes allow much larger time steps even if the elements of these meshes are of "bad quality" in the common sence. Hence, it is important to consider the quality of the mesh *in relation to the diffusion* and not on itself.

5 Conclusions

Theorem 3.3 gives an easily computable bound on the largest eigenvalue of the system matrix $\tilde{M}^{-1}A$ in terms of the diagonal entries of $\tilde{M}$ and A with $\tilde{M}$ being either M or M_{lump}. The bound is tight for *any mesh* and *any diffusion matrix* $\mathbb{D}$ within a small constant which is given explicitly and depends only on the dimension of the domain. This allows efficient and accurate estimation of the largest permissible time step $\tau_{\max}$.

Moreover, estimates (38) and (40) in terms of the mesh geometry reveals how the mesh and the diffusion matrix affect the stability condition. Roughly speaking, $\tau_{\max}$ depends only on the number of mesh elements and the matching between the element geometry with the diffusion matrix. Thus, it is not the element geometry itself but the *element geometry in relation to the diffusion matrix* that is important for the stability. The element quality measure $\mathrm{Q}_{\mathbb{D}^{-1}}$ provides a measure for the effect of a given element on the stability condition. As seen in Example 4.2, strong anisotropic adaptation in the "wrong" direction can cause a significant reduction of the time step size. Meanwhile, the result suggests that improvements in the element quality can significantly increase $\tau_{\max}$.

Furthermore, numerical results suggest that, at least in one and two dimensions, mass lumping can increase the time step size by a factor of 2 to 3. This topic deserves more detailed

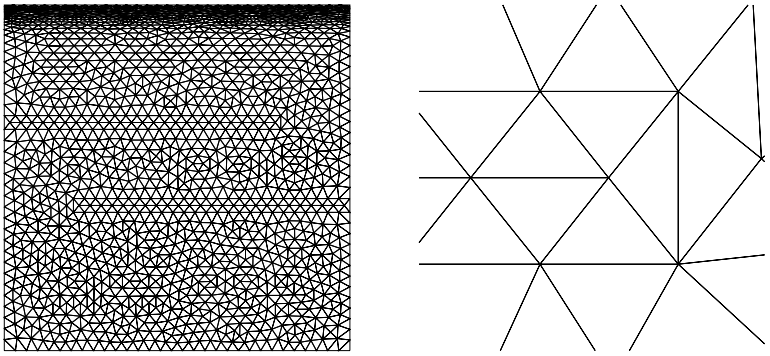

(a) $t = 1.0\times10^2$, $N = 3\,071$

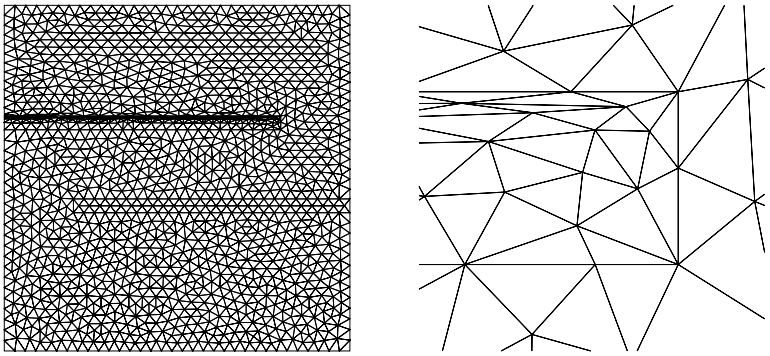

(b) $t = 5.0\times10^3$, $N = 2\,799$

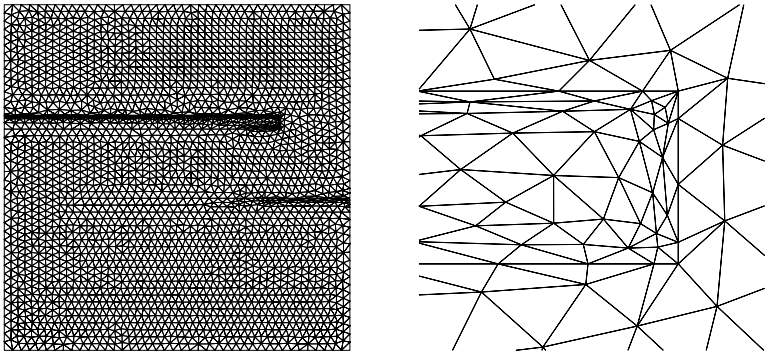

(c) $t = 1.0\times10^4$, $N = 5\,305$

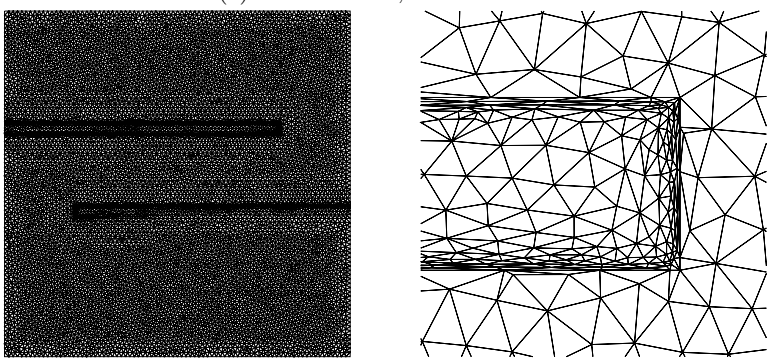

(d) $t = 1.0\times10^5$, $N = 20\,334$

Figure 5: Mesh examples and close-ups at $[74, 82] \times [62, 70]$ (the upper right corner at the entrance of the tunnel) for the ground water flow example (Example 4.3)

Table 5: Anisotropic diffusion example (Example 4.4)

(a) quasi-uniform meshes (without mass lumping)

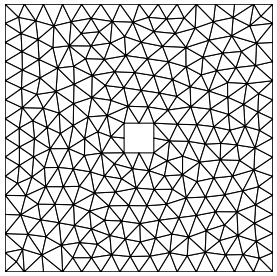

		estimate (39)		estimate (42)	
N	$\tau_{\max}/s^2$	τ_h/s^2	$\tau_{\max}/\tau_h$	τ_h/s^2	$\tau_{\max}/\tau_h$
2 094	2.95×10^{-7}	1.57×10^{-8}	18.87	8.98×10^{-9}	32.89
7 720	7.59×10^{-8}	4.68×10^{-9}	16.21	2.18×10^{-9}	34.84
27 274	2.21×10^{-8}	1.34×10^{-9}	16.51	6.24×10^{-10}	35.40
93 518	5.28×10^{-9}	2.65×10^{-10}	19.89	1.49×10^{-10}	35.49

(b) $\mathbb{D}^{-1}$-uniform meshes (without mass lumping)

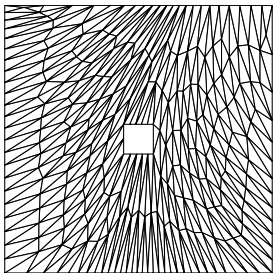

		estimate (39)		estimate (42)	
N	$\tau_{\max}/s^2$	τ_h/s^2	$\tau_{\max}/\tau_h$	τ_h/s^2	$\tau_{\max}/\tau_h$
2 131	9.82×10^{-7}	1.27×10^{-7}	7.72	1.71×10^{-10}	5 753.02
7 703	3.83×10^{-7}	3.64×10^{-8}	10.51	5.17×10^{-11}	7 410.76
27 285	1.67×10^{-7}	1.58×10^{-8}	10.57	2.98×10^{-11}	5 611.08
93 799	6.20×10^{-8}	6.10×10^{-9}	10.16	8.05×10^{-12}	7 698.00

investigations.

Finally, it is worth pointing out that the analysis presented in this work applies to other explicit time integration schemes with polynomial stability functions, such as extrapolation methods.

References

[DWZ09] Q. Du, D. Wang, and L. Zhu. "On mesh geometry and stiffness matrix conditioning for general finite element spaces." In: *SIAM J. Numer. Anal.* 47.2 (2009), pp. 1421–1444.

[ELR02] B. Erdmann, J. Lang, and R. Roitzsch. *KARDOS - User's Guide*. ZIB-Report 02-42. `http://www.zib.de/de/numerik/software/kardos.html`. ZIB, 2002.

[Fri73] I. Fried. "Bounds on the spectral and maximum norms of the finite element stiffness, flexibility and mass matrices." In: *Internat. J. Solids and Structures* 9 (1973), pp. 1013–1034.

[GM06] I. G. Graham and W. McLean. “Anisotropic mesh refinement: the conditioning of Galerkin boundary element matrices and simple preconditioners.” In: *SIAM J. Numer. Anal.* 44.4 (2006), 1487–1513 (electronic).

[GP13] J.-L. Guermond and R. Pasquetti. “A correction technique for the dispersive effects of mass lumping for transport problems.” In: *Comput. Methods Appl. Mech. Engrg.* 253 (2013), pp. 186–198.

[HW96] E. Hairer and G. Wanner. *Solving ordinary differential equations. II*. Second. Vol. 14. Springer Series in Computational Mathematics. Stiff and differential-algebraic problems. Berlin: Springer-Verlag, 1996.

[Hec] F. Hecht. *BAMG: bidimensional anisotropic mesh generator*. `http://www.ann.jussieu.fr/hecht/ftp/bamg/`.

[Hua05a] W. Huang. “Measuring mesh qualities and application to variational mesh adaptation.” In: *SIAM J. Sci. Comput.* 26.5 (2005), 1643–1666 (electronic).

[Hua05b] W. Huang. “Metric tensors for anisotropic mesh generation.” In: *J. Comput. Phys.* 204.2 (2005), pp. 633–665.

[Hua07] W. Huang. “Anisotropic mesh adaptation and movement.” In: *Adaptive computations: Theory and Algorithms*. Ed. by T. Tang and J. Xu. Mathematics Monograph Series 6. Science Press, Beijing, 2007. Chap. 3, pp. 68–158.

[HR11] W. Huang and R. D. Russell. *Adaptive Moving Mesh Methods*. Vol. 174. Applied Mathematical Sciences. New York: Springer, 2011.

[KHX] L. Kamenski, W. Huang, and H. Xu. *Conditioning of finite element equations with arbitrary anisotropic meshes*. In: *Math. Comp.* (forthcoming). arXiv:`1201.3651`.

[LH10] X. Li and W. Huang. “An anisotropic mesh adaptation method for the finite element solution of heterogeneous anisotropic diffusion problems.” In: *J. Comput. Phys.* 229.21 (2010), pp. 8072–8094.

[MP08] S. Micheletti and S. Perotto. “Anisotropic mesh adaption for time-dependent problems.” In: *Int. J. Numer. Meth. Fluids* 58.9 (2008), pp. 1009–1015.

[PS12] D. Peterseim and S. A. Sauter. “Finite elements for elliptic problems with highly varying, nonperiodic diffusion matrix.” In: *Multiscale Model. Simul.* 10.3 (2012), pp. 665–695.

[Wat87] A. J. Wathen. “Realistic eigenvalue bounds for the Galerkin mass matrix.” In: *IMA J. Numer. Anal.* 7.4 (1987), pp. 449–457.

[ZD11] L. Zhu and Q. Du. “Mesh-dependent stability for finite element approximations of parabolic equations with mass lumping.” In: *J. Comput. Appl. Math.* 236.5 (2011), pp. 801–811.

[ZD14] L. Zhu and Q. Du. “Mesh dependent stability and condition number estimates for finite element approximations of parabolic problems.” In: *Math. Comp.* 83.285 (2014), pp. 37–64.